# Electrocatalytic Water Oxidation at Neutral pH by a Nanostructured $Co(PO_3)_2$ Anode

*Hyun S. Ahn and T. Don Tilley**

**Cobalt metaphosphate $Co(PO_3)_2$ nanoparticles are prepared via the thermolytic molecular precursor (TMP) method. A Ni form electrode decorated with $Co(PO_3)_2$ nanoparticles is evaluated as an anode for water oxidation electrocatalysis in pH 6.4 phosphate-buffered water. Catalytic onset occurs at an overpotential of ca. 310 mV, which is 100 mV lower than that observed for $Co_3O_4$ nanoparticles, with a comparable surface area under identical conditions. A per-metal turnover frequency (TOF) of 0.10–0.21 $s^{-1}$ is observed at an overpotential, $\eta$, of 440 mV, which is comparable to the highest rate reported for a first-row metal heterogeneous catalyst. Post-catalytic characterization of the catalyst resting state by X-ray photoelectron spectroscopy (XPS) and Raman spectroscopy reveals that surface rearrangement occurs, resulting in an oxide-like surface overlayer.**

## 1. Introduction

There is growing interest in development of environmentally benign means for the conversion of solar energy to chemical energy in the form of transportable, storable fuels.[1] Potentially viable artificial photosynthetic systems might involve the oxidation of water to yield oxygen and protons, which may then be employed in an electrocatalytic reduction to produce a chemical fuel (e.g., $H_2$, $CH_4$, $CH_3OH$, etc.). A key technical challenge for enabling such systems is the discovery of efficient catalysts for the oxidative half-reaction that splits water to oxygen and protons. Molecular and heterogeneous catalysts have been developed for this reaction, and many of the most promising results have been provided by compounds and oxides of iridium and ruthenium.[2–10] However, the large-scale application of artificial photosynthesis should be based on less expensive, more abundant metals such as manganese, iron and cobalt.[11–22] Along these lines, considerable attention is being focused on materials and compounds of these metals, and particular interest in cobalt was sparked by a recent report by Nocera and coworkers on a cobalt phosphate material containing oxy-hydroxide layers that operates as an electrocatalytic water-splitting catalyst under neutral pH.[12] Especially given the different electrochemical and chemical properties of this material with respect to those of simple oxides of cobalt such as $Co_3O_4$ and CoO, it is of interest to investigate additional cobalt materials that incorporate inorganic anions other than oxide.[12,15]

This laboratory has had a long-standing interest in the use of single-source molecular precursors for the synthesis of materials with well-defined stoichiometries. This approach, termed the thermolytic molecular precursor (TMP) method, allows synthetic control over a material's phase, composition, and nanostructure.[23] It may be employed in solid- and solution-state transformations to materials, and is amenable to solution processing at low temperatures.[23–26] Previous investigations in this area have targeted phosphate materials of zinc[23b,25d,27,28] and aluminum[23e,25d–e,27–29] with precursor metal complexes of the $-O_2P(OtBu)_2$ ligand. Well-defined molecular precursors to cobalt phosphate materials are rare, but examples have been reported by Murugavel and coworkers, for conversion to the cobalt phosphates $Co(PO_3)_2$ and $Co_2P_2O_7$.[25a,c] Given the interest in cobalt phosphate materials of controlled stoichiometry and structure, it seems that the TMP approach may provide routes to new water oxidation catalysts with tailored properties.

Herein, we report a nanostructured cobalt metaphosphate material, derived from thermal processing of a molecular precursor, as an electrocatalyst for water oxidation. This nanostructured cobalt metaphosphate catalyst $Co(PO_3)_2$ displays improved stability in neutral pH relative to cobalt oxide, and surpasses it in per-metal efficiency by an order of magnitude at pH 6.4 while exhibiting a lower onset overpotential.

## 2. Results and Discussion

### 2.1. Synthesis of $Co(PO_3)_2$ from the Single-Source Molecular Precursor $\{Co[O_2P(O^tBu)_2]_2\}_n$ (1)

The polymeric precursor complex $\{Co[O_2P(O^tBu)_2]_2\}_n$ (**1**) was synthesized in high yield by a modification of the literature procedure,[25c] from $CoCl_2 \cdot 6H_2O$ and $KO_2P(O^tBu)_2$ in acetonitrile. The UV-vis spectrum of **1** (Figure S1, Supporting Information) is consistent with the presence of Co(II) in a pseudo-tetrahedral environment,[34] and the reported X-ray crystal structure reveals polymeric chains of Co(II) centers

H. S. Ahn, Prof. T. D. Tilley
Department of Chemistry
University of California, Berkeley
Berkeley, CA 94720, USA
E-mail: tdtilley@berkeley.edu
H. S. Ahn, Prof. T. D. Tilley
Chemical Sciences Division
Lawrence Berkeley National Laboratory
1 Cyclotron Road, Berkeley, CA 94720, USA

DOI: 10.1002/adfm.201200920

bridged alternately by three and then one–$O_2P(O^tBu)_2$ ligand. Compound **1** has not been investigated as a thermolytic precursor to cobalt-based materials, but the related tetra-cobalt species $Co_4(\mu_4\text{-}O)[O_2P(O^tBu)_2]_6$ was shown by Murugavel and co-workers to thermally decompose at 350 °C to amorphous $Co_4P_6O_{19}$, which then converts at 850 °C to a mixture of $Co(PO_3)_2$ and $Co_2P_2O_7$.[25a,c]

Compound **1** serves as a low-temperature precursor to cobalt metaphosphate, $Co(PO_3)_2$ (vide infra), due to the facile thermal elimination of isobutene from the di-*tert*-butyl phosphate ligand.[23] As observed by thermal gravimetric analysis (TGA, Figure S6, Supporting Information), precursor **1** undergoes clean thermolysis under a stream of air, with a sharp mass loss of ca. 50% at 138 °C. The final ceramic yield was 44.4%, which closely corresponds to the calculated yield for $Co(PO_3)_2$ of 45.4%. The identity of the material after thermolysis was confirmed by powder X-ray diffraction (PXRD, Figure S7, Supporting Information).[35] This thermolytic decomposition behavior is quite similar to that of the analogous zinc precursor $\{Zn[O_2P(O^tBu)_2]_2\}_n$.[23b] Structural transformations during thermolysis are not apparent by differential scanning calorimetry (DSC, Figure S5, Supporting Information), which reveals no significant features to 600 °C, suggesting that oxide formation and phase separation are unlikely. Characterization of the material by PXRD, UV-Vis spectroscopy, and Raman spectroscopy revealed no evidence for other structures, e.g., oxides or phosphates of cobalt (see Supporting Information).

For use of precursor **1** in the preparation of $Co(PO_3)_2$, solution-based methods were investigated as routes to nanoparticles, which should provide a high surface area for the electrocatalytic anode material. Thermal decomposition of a precursor solution in a pressure vessel was selected as the method of catalyst preparation based on the desired properties of the material to be used in electrocatalysis (i.e., high surface area and ease of electrode fabrication). An ethanol solution of precursor **1** (0.5 mM, 15 mL) was placed in a 25 mL pressure reactor, which was then positioned in an oven preset at 240 °C. The thermal decomposition process is illustrated in Equation 1.

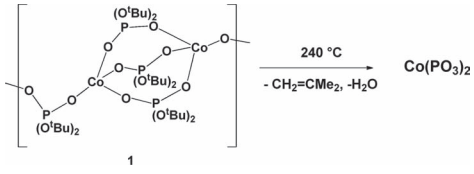


1 (1)

After 12 h, a blue powder that separated from solution was washed with water and acetone, to provide a quantitative yield of nanostructured $Co(PO_3)_2$. The isolated material exhibited a web-like morphology (**Figure 1**) with an appreciable surface area (20–30 $m^2/g$), and was readily dispersed in an alcohol solvent for solution depositions onto a Ni-foam electrode surface. In a typical electrode fabrication, a 1 mg/mL dispersion of $Co(PO_3)_2$ in ethanol or isopropanol was drop-cast onto Ni-foam (area 1 $cm^2$) or glassy carbon (3 mm diameter, 0.07 $cm^2$ area) electrodes. Materials with a higher surface area (up to 160 $m^2/g$) were synthesized by addition of a surfactant (e.g., cetrimonium bromide, and Pluronic P123) to the precursor solution prior to thermolysis. However, the resulting materials generally exhibited larger individual (and presumably porous) particles that were difficult to incorporate onto the surface of an electrode.

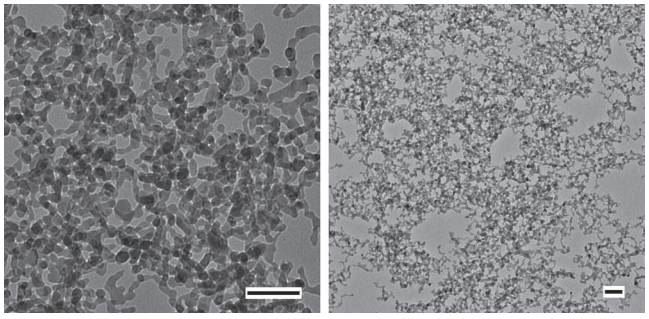

**Figure 1.** Typical transmission electron microscopy image of web-like $Co(PO_3)_2$. Both scale bars are 100 nm.

### 2.2. Electrocatalytic Water Oxidation with $Co(PO_3)_2$ Nanoparticles

Electrochemical experiments including linear sweep voltammetry (LSV), cyclic voltammetry (CV), and controlled potential electrolysis (CPE) were performed in a two-compartment H-cell with a three-electrode configuration in 0.1 M phosphate-buffered solution with a measured pH of 6.4. Similar electrocatalytic results (vide infra) were obtained in acetate buffer at pH 5.6; however, the $Co(PO_3)_2$ catalyst exhibited instability in strongly acidic and basic conditions (pHs lower than 3 and higher than 11). The working electrodes consisted of the catalyst particles deposited onto Ni foam (scanning electron microscopy image shown in Figure S8, Supporting Information) or glassy carbon, which were used in combination with a polished platinum wire counter electrode and a Ag/AgCl reference electrode. Over the potential range investigated (up to 1.1 V vs. Ag/AgCl), the Ni foam electrode exhibits no discernible features (**Figure 2**), such that background corrections were unnecessary, as determined previously in studies with $Co_3O_4$ nanoparticles.[18] No background correction was applied for electrolysis on the glassy carbon electrode, as it also exhibited no discernible features in the potential range investigated (Figure S10, Supporting Information).

As seen in the cyclic voltammogram of the cobalt metaphosphate catalyst on Ni foam (Figure 2), the $Co^{II}/Co^{III}$ and the $Co^{III}/Co^{IV}$ transitions (at ca. 0.7–1.0 V vs. Ag/AgCl) commonly observed prior to catalytic water oxidation[12,18,19] were not well resolved at scan rates higher than 10 mV/s. However, this transition was partially resolved in LSV experiments at a low scan rate of 1 mV/s (Figure S9, Supporting Information). From this scan, a charge integration of the presumed $Co^{II}/Co^{III}$ and $Co^{III}/Co^{IV}$ transitions corresponds to ca. four times the number of cobalt atoms in the sample. This appears to be due to the fact that this oxidation is not cleanly separated from water oxidation, unlike in the case of $Co_3O_4$, and this is consistent with the observed lower onset potential for $Co(PO_3)_2$ (vide infra). A similar superpositioning of catalyst and water oxidation was observed for catalyst deposited on glassy carbon electrodes (Figures S10 and S11, Supporting Information).

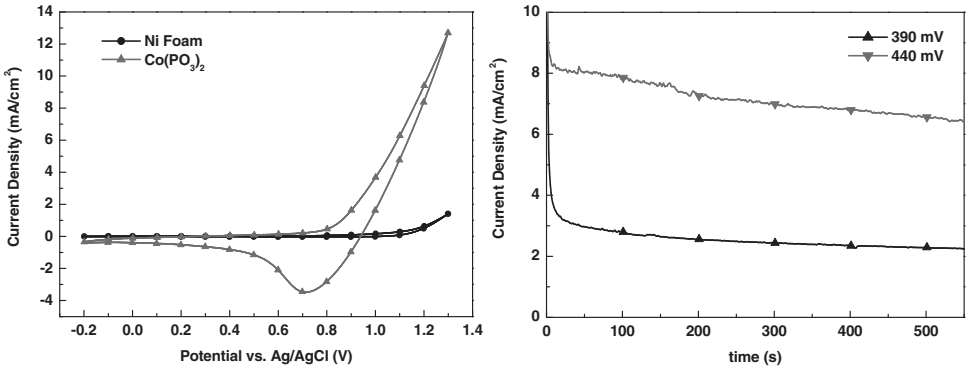


**Figure 2.** Cyclic voltamogram of nanostructured $Co(PO_3)_2$ at a scan rate of 100 mV/s (left). The CV of blank Ni foam is shown as a reference. Current evolution over time by CPE at overpotentials of 390 mV and 440 mV is shown on the right. The slight drop in current density over time is due to loss of surface area by bubble formation.

To further examine the onset of electrocatalytic water oxidation for this material, LSV on a flat glassy carbon electrode was utilized at 1 mV/s scan rate. As seen in **Figure 3**, catalytic current was observed at ca. 0.95 V vs. Ag/AgCl, along with vigorous oxygen bubble formation. Note that the oxidative feature occurring at ca. 0.86 V is the oxidation of the catalyst preceding water oxidation. The catalytic onset potential for the nanostructured $Co(PO_3)_2$ catalyst was determined by the intercept of lines extrapolated from the exchange current and catalysis current in the high overpotential (Tafel) region (see Supporting Information for detailed calculations). The onset overpotential determined by this method was 313 mV, which is significantly lower than those associated with $Co_3O_4$ and CoPi (vide infra). The onset potential for a Ni foam electrode decorated with nanostructured $Co(PO_3)_2$ was estimated by measuring steady state currents by CPE at incremental potentials (240 mV to 440 mV in 10 mV increments, Table S1, Supporting Information). The resulting overpotential of ca. 300 mV is in good agreement with that determined from a glassy carbon electrode. An overpotential of ca. 310 mV for the onset of water oxidation catalysis is low for a cobalt-based system.[12–19]

For direct comparisons, the same electrochemical experiments were conducted with $Co_3O_4$ nanoparticles[33] of a similar surface area (d = ca. 20 nm by TEM, BET surface area = 25 $m^2/g$), and with the cobalt phosphate thin film catalyst (CoPi) described by Nocera and coworkers.[12a] A cyclic voltammogram comparing the electrocatalytic behavior of all three catalysts on Ni foam is shown in Figure 3. The three systems exhibit distinct electrocatalytic behaviors, indicating that despite possible similarities in the composition of the surface layer, the catalytically active sites appear to be distinctly different under oxidizing potentials. Comparisons of the three electrode materials described here must be made on the basis of surface areas, because in general electrocatalytic activity exhibits a strong correlation to the electrode surface area.[18a] The three electrodes compared here were prepared such that their electrochemically active surface areas, as determined by double layer capacitance measurements, were very similar (see Supporting Information).[36] Scanning electron microscopy (SEM) images of $Co(PO_3)_2$ and $Co_3O_4$ particles on Ni foam (Figure S8, Supporting Information) reveal similar surface coverages by the respective nanoparticles, corroborating similarities in the capacitances observed electrochemically.

Catalytic onsets for the $Co_3O_4$ and CoPi catalysts were also determined from the Tafel and exchange current data (Figure 3; Figure S11 and Table S1, Supporting Information). The onset potentials determined in this way, for the $Co_3O_4$ nanoparticles and the CoPi catalyst, were 414 mV and 434 mV, respectively (100–120 mV greater than that achieved by the cobalt

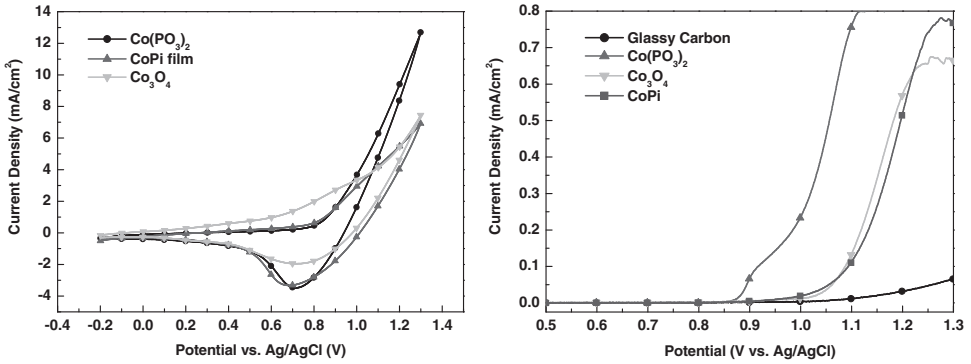


**Figure 3.** Comparison of CVs of three different materials at a scan rate of 100 mV/s (left). All of them were deposited on Ni foam and the sample loadings were 0.9 mg for $Co_3O_4$, 1.1 mg for $Co(PO_3)_2$, and 1.2 mg for the CoPi catalyst. LSV of the catalysts in comparison are shown on the right. Catalytic onset of the nanostructured $Co(PO_3)_2$ catalyst at a significantly lower potential was observed. The nonlinearity of the catalytic current at high overpotentials is due to large changes in the electrode area arising from vigorous bubble formation.

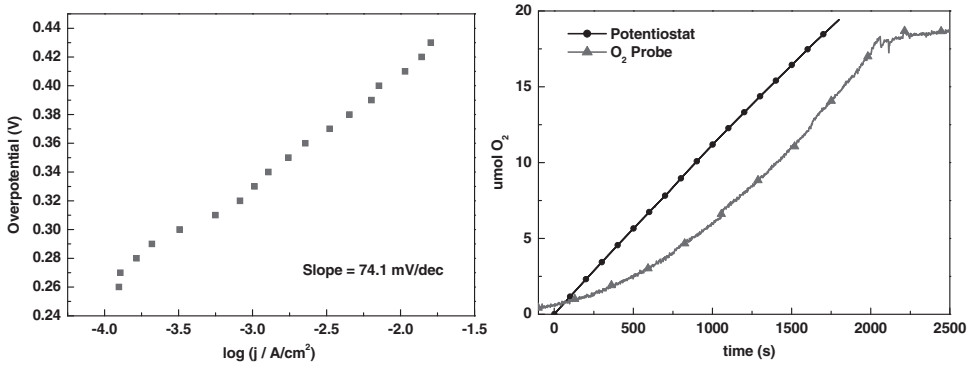


**Figure 4.** Tafel plot of $Co(PO_3)_2$ (left), with a slope of 74.1 mV/dec ($\eta$ = applied voltage–thermodynamic potential). A test of Faradic efficiency by simultaneous detection of headspace $O_2$ with CPE is presented on the right. Faradaic efficiencies of 98 ± 4% were recorded over multiple experiments. The time lag between the two curves is due to adhesion of bubbles on the porous electrode, giving rise to detection delay by the probe in the reactor headspace.

metaphosphate catalyst). A shift of ca. 100 mV in the onset potential is significant, and implies that the nanostructured $Co(PO_3)_2$ catalyst is inherently more efficient.

Prolonged catalytic activities at higher overpotentials ($\eta \geq$ 300 mV) were also investigated by CPE on a Ni foam electrode. Sustained current densities of 0.17, 0.62, 3.30, and 8.01 mA/cm$^2$ (based on projected electrode surface area) were recorded at $\eta$ = 300, 340, 390, and 440 mV, respectively (Figure 2 and Figure S12, Supporting Information), over at least 8 h. Despite fluctuations in the electrode areas due to excessive bubble formation, several mA of current was observed at moderate overpotentials, which indicates rapid catalysis. A per-metal turnover frequency (TOF) range for the catalyst was calculated from the current densities obtained via CPE and the number of surface sites estimated from the known crystal structures for $Co(PO_3)_2$ and $Co_3O_4$, the latter of which more closely models the surface active species (vide infra) and represents a higher density of surface-exposed cobalt atoms (see Supporting Information for detailed calculations). From these measurements, TOF ranges of the cobalt metaphosphate catalyst were determined to be 0.002–0.005, 0.008–0.016, 0.044–0.086, and 0.10–0.21 s$^{-1}$ at $\eta$ = 300, 340, 390, and 440 mV, respectively. These TOF values are higher than those of most cobalt-based water oxidation catalysts operating at similar overpotentials, and an order of magnitude higher than that of $Co_3O_4$ nanoparticles of similar surface area at pH 6.4.[12–19] The $Co(PO_3)_2$ anode was reevaluated using CV and LSV methods after 1 h of catalysis at 440 mV overpotential, and the voltammograms (both CV and LSV) were unchanged, indicating that the electrochemical behavior was not altered during catalysis. It is worth noting that the nanostructured $Co(PO_3)_2$ catalyst decomposed in strongly acidic and basic conditions (pHs lower than 3 and higher than 11), whereas long-term stability of $Co_3O_4$ under water oxidation conditions in basic solutions has been reported.[17–19] Different catalysts are associated with characteristic pH ranges for which optimal catalytic performance and stability is observed, and the nanostructured $Co(PO_3)_2$ catalyst is most effective at near neutral pHs.

Oxygen detection experiments were conducted to determine the Faradaic efficiencies associated with the catalytic current. Electrolysis experiments were conducted in a gas-tight H-cell, while the headspace oxygen concentration was monitored by a multi-frequency fluorescence oxygen probe. Faradaic efficiencies of 98 ± 4% were obtained at $\eta$ = 440 mV, indicating that within experimental error all of the current is consumed for oxygen evolution (**Figure 4**).

The high overpotential (Tafel) region of the current-voltage plot is shown in Figure 4. The Tafel slope for the $Co(PO_3)_2$ catalyst is 74.1 mV/dec, suggesting that it operates by a mechanism similar to that of metal oxides. The actual Tafel slope may be lower, since the electrode surface area is reduced during catalysis by bubble formation. Attempts to make similar measurements on $Co_3O_4$ nanoparticles were unsuccessful due to the limited stability of this material at the experimental pH of 6.4.[17]

### 2.3. Post-Catalytic Characterization of the Catalyst

To investigate structural changes associated with the electrocatalysis, the catalysts were examined after catalytic runs. Raman spectroscopy was performed on the catalyst prior to application of an oxidizing bias, and again after a potential of 1.1 V (vs. Ag/AgCl) had been applied over the course of one hour (**Figure 5**). Before electrocatalysis, the Raman spectrum exhibited only bands attributed to cobalt metaphosphate at 475, 665, 980, and 1095 cm$^{-1}$ (Figure 5).[38] After catalysis, Raman bands for the metaphosphate are less prominent, and a broad feature at 597 cm$^{-1}$, assigned to Co-O stretches, indicates the presence of surface $CoO_x$ species.[39]

Given the similar compositions of the CoPi and $Co(PO_3)_2$ catalysts, it was of interest to compare their structural features after catalysis. The post-catalytic Raman spectra of these catalysts exhibit distinct differences (Figure 5). Weak and broad bands at ca. 550 and 620 cm$^{-1}$ are observed for the CoPi catalyst, similar to Co-O stretches seen in $Co_3O_4$.[17,39c] Note that the surface-bound active sites for the CoPi catalyst are thought to consist of cubane-like cobalt oxide clusters, as evidenced by X-ray absorption spectroscopy.[12e,f] The most distinctive feature in the post-catalytic $Co(PO_3)_2$ sample is a broad peak at 597 cm$^{-1}$, which has previously been assigned to the presence of amorphous $CoO_x$ species.[39] Diminishment of the peak at 980 cm$^{-1}$ due to $PO_4^{3-}$ tetrahedral is also consistent with surface enrichment by $CoO_x$ layer species (vide infra). Thus, the active surface species in this material may be small $CoO_x$ domains, perhaps similar to those associated with the CoPi catalyst, supported by the underlying

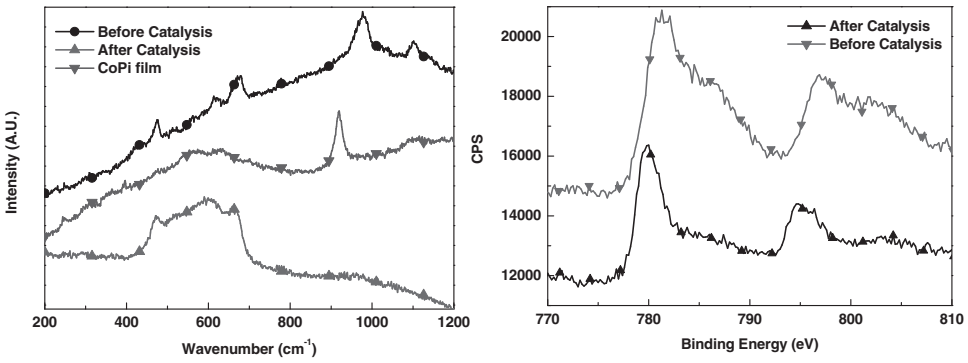


**Figure 5.** Raman spectra of $Co(PO_3)_2$ as synthesized and after being utilized in catalysis are displayed alongside that of the CoPi film catalyst (left). The cobalt 2p region of the XPS spectrum of $Co(PO_3)_2$ prior to and after catalysis exhibits diminished shoulder peaks due to the oxidation of cobalt centers (right).

$Co(PO_3)_2$ structure. The distinct differences in the electrocatalytic behaviors for the CoPi and $Co(PO_3)_2$ catalysts (vide supra) may therefore be attributed to the influence of active site-support interactions, which may lead to different structures for the surface-bound sites under catalytic conditions.

Evidence for cobalt oxide species in the post-catalytic material was also found by X-ray photoelectron spectroscopy (XPS, Figure 5 and Figure S13, Supporting Information). Prior to catalysis, $2p_{1/2}$ and $2p_{3/2}$ XPS peaks for Co at 780.0 and 795.2 eV, with broad shoulders at 786.0 and 801.6 eV, are observed (Figure 5). The broad shoulder features indicate that most of the Co centers of the $Co(PO_3)_2$ nanoparticles are in the Co(II) oxidation state.[40,41] After catalysis, the shoulder peaks at 786.0 and 801.6 eV are greatly diminished, indicating that most of the Co centers detected had been converted to higher oxidation states.[40] Analysis of the post-catalytic material by XPS also indicates the presence of phosphate at or near the surface, as shown by a phosphorous 2p peak at 133 eV (Figure S13, Supporting Information).[38] The stoichiometry of the post-catalysis material was estimated by integration of the XPS spectrum, which gave a Co:P:O ratio of 4:1:9.9 (Table S2, Supporting Information). These values reflect enrichment of cobalt and oxygen at the surface; for comparison the measured ratio for pre-catalytic $Co(PO_3)_2$, determined by XPS analysis, is 1:1.9:6.8. These results from Raman and XPS studies are consistent with a restructuring of the surface with formation of oxide-like species during electrocatalysis. The Pourbaix diagram for Co in phosphate-buffered solutions[15b,42] suggest that $Co(PO_3)_2$ nanoparticles will not be completely stable under electrocatalytic conditions at pH 6.4, and that surface formation of $Co(OH)_2$ should occur, followed by conversion to oxide species under an oxidizing bias. The post-catalytic material was examined by several methods. Analysis by XRD proved difficult due to strong attachment of the catalyst particles onto the electrode. Inductively coupled plasma optical emission spectroscopy (ICP-OES) revealed that the cobalt and phosphorous compositions were 27.7 and 28.4 wt%, respectively, in agreement with the expected composition of $Co(PO_3)_2$ (27.2 wt% Co and 28.6 wt% P). A negligible incorporation of potassium from the buffer solution (0.7 wt%) also suggests that the transformation to an oxide-like species occurs only at the surface while the bulk $Co(PO_3)_2$ structure remains. The post-catalytic material also exhibits the Raman peak at 665 $cm^{-1}$ (Figure 3), characteristic of $Co(PO_3)_2$ and previously assigned to a symmetric stretching frequency for bridging P-O groups in long-chain polyphosphates.[38a] This also suggests that the underlying $Co(PO_3)_2$ structure is unaltered during catalysis and surface transformations.

It should be noted that the oxide species observed by Raman spectroscopy and XPS, detected without applied potential, are likely not those directly involved in catalysis. Under the oxidizing potentials used for catalysis, the Pourbaix diagram of cobalt in phosphate-buffered water[15b,42] predicts the formation of high oxidation state species such as $CoO_2$ and $Co(OH)_3$. Similar chemical species, presumed to be present at the surface of the $Co(PO_3)_2$-based anode during catalysis, may then transform in the absence of the oxidizing bias to the cobalt oxide species detected by spectroscopy. Surface rearrangement phenomena in $Co_3O_4$ and CoPi water oxidation systems have been investigated by various researchers, and the formation of a double layer, hydroxide-type structure, Co(O)OH, has been observed by Raman and X-ray absorption spectroscopies.[12e,15b,17] It is likely that a similar surface transformation is occurring in the nanostructured $Co(PO_3)_2$ catalyst, based on the Raman and XPS data. However, given the distinct behavior of the nanostructured $Co(PO_3)_2$ catalyst (in terms of catalytic rate and onset overpotential), it is possible that the observed enhancement is due to a synergistic effect of the underlying $Co(PO_3)_2$ structure on the catalytically active surface $CoO_x$ species. In situ vibrational and X-ray absorption spectroscopies should further reveal the structure of the active species, and such experiments are planned for the near future.

## 3. Conclusions

The studies described above demonstrate a convenient molecular precursor route to nanostructured cobalt metaphosphate materials. In addition, nanoparticles of $Co(PO_3)_2$ have been shown to function as an electrocatalyst for water oxidation, at a relatively low overpotential of about 310 mV. A per-metal turnover frequency of 0.10–0.21 $s^{-1}$ at $\eta$ = 440 mV is comparable to the highest rate reported for a first-row metal heterogeneous system for water oxidation,[11–19,21c,22] and this represents a substantially higher rate than that observed for $Co_3O_4$ and CoPi catalysts of similar surface areas at pH 6.4 (0.011 and 0.0026 $s^{-1}$, respectively, at similar overpotentials).[12d,43]

Spectroscopic studies indicate that the surface of the $Co(PO_3)_2$-based electrocatalyst undergoes restructuring during electrocatalysis, resulting in bound $CoO_x$ species supported by the underlying $Co(PO_3)_2$ structure. The anion in the catalyst material, as well as the nature of the interaction between the catalytic, surface-bound species and the support material appear to play roles in water oxidation catalysis, as evidenced by the distinct electrocatalytic behaviors observed for $Co_3O_4$, CoPi, and $Co(PO_3)_2$. Thus, investigations of cobalt-based inorganic materials with a range of anions should help to develop structure-function relations and point the way to more efficient catalysts.

## 4. Experimental Section

*General*: Nitrogen adsorption isotherms were obtained using a Quantachrome Autosorb 1, with samples outgassed at 120 °C for at least 20 h prior to data collection. The BET method was used for surface area determination and the BJH method was used for pore size distribution calculations.[30,31] TGA-DSC measurements were conducted using a Seiko Exstar6000 brand TG/DTA6300 analyzer coupled to a Pfeiffer Thermostar mass spectrometer. Carbon, hydrogen, and nitrogen elemental analyses were performed at the College of Chemistry microanalysis laboratory at the University of California, Berkeley. DR-FTIR spectra were obtained on a Mattson FTIR spectrometer. The DRUV-Vis spectrum was acquired using a Perkin-Elmer Lambda 9 spectrometer equipped with a 60 mm integrating sphere, a slit width of 4 nm, and at a collection speed of 120 nm/min. Samples were run using MgO as a reference background. Powder X-ray diffraction (PXRD) patterns were recorded on a Bruker D-8 GADDS X-ray diffractometer using Co K$\alpha$ radiation ($\lambda$ = 1.7902 Å). pH measurements were conducted using a Thermo Orion 2 star pH meter. Electrochemical data were recorded on a Bioanalytical Systems model EC epsilon computer-controlled potentiostat. Unless otherwise stated, all measurements were conducted in a two-compartment H-cell with a three-electrode configuration. Electrochemistry experiments were performed on solutions buffered with 0.1 M phosphate ($NaH_2PO_4/Na_2HPO_4$ measured pH of 6.4) referenced to a Ag/AgCl reference electrode. Ag/AgCl electrodes were calibrated relative to Potassium Ferricyanide in order to correct for any potential drifts. Solution resistance in CV and LSV experiments was corrected for by the iR compensation algorithm, using software in the EC epsilon potentiostat. Polished platinum wire was used as an auxiliary electrode, and catalyst deposited onto Ni foam or glassy carbon was used as a working electrode. The catalyst was loaded onto the Ni foam by drop-casting of a 1 mg/mL solution (in ethanol) to achieve a loading of 1 ± 0.1 mg/cm$^2$ (confirmed by determining the change in mass with an analytical balance). For electrolysis on a flat electrode, glassy carbon with a 3 mm diameter was utilized, also by drop-casting catalysts. Transmission electron microscopy (TEM) was performed on a Hitachi H-7650 TEM operating at 120 kV. Scanning electron microscopy (SEM) was performed on a JEOL Field Emission SEM operating at 5 kV. Raman experiments were performed on an epi-illumination confocal Raman microscope (LabRam HR, Horiba Jobin, Yvon) with HeNe laser (1 mW) at 633 nm as an excitation source. Inductively coupled plasma optical emission spectroscopy (ICP-OES) for cobalt ion detection in post catalytic solutions was performed on a Perkin-Elmer ICP-OES Optima 7000 DV. Standard solutions were purchased from Perkin-Elmer and used as received. X-ray photoelectron spectroscopy (XPS) was performed on a Perkin-Elmer PHI 5300 ESCA system with a Mg anode driven at 100 W. The compound $KO(O)P(O^tBu)_2$ was prepared according to literature procedures.[32] Cobalt oxide ($Co_3O_4$) nanoparticles used in comparison experiments were prepared according to literature procedures.[33] The CoPi water oxidation catalyst was prepared according to a literature procedure,[12a] via direct deposition onto the electrode substrate.

*Synthesis of* $\{Co[O_2P(O^tBu)_2]_2\}_n$ **(1)**: The synthesis of $\{Co[O_2P(O^tBu)_2]_2\}_n$ was conducted using a modified preparation reported by Murugavel et al.[25a,25c] In a typical synthesis, $KO(O)P(O^tBu)_2$ (4.97 g, 20 mmol) was dissolved in acetonitrile (ca. 25 mL). An acetonitrile (15 mL) solution of $CoCl_2{\cdot}6H_2O$ (2.38 g, 10 mmol) was then added. An instant color change to blue and precipitation of KCl was observed. Product was obtained in greater than 80% yield by crystalization from slowly evaporating diethyl ether under $N_2$. Anal. Calcd: C, 40.26; H, 7.60; Co, 12.34. Found: C, 40.13; H, 7.82; Co, 12.11. IR (DRIFTS, KBr, cm$^{-1}$) 1564 (m), 1419 (w), 1375 (w), 1367 (m), 1191 (m), 1174 (s), 1072 (s), 993 (m), 916 (w), 831 (w), 700 (w), 547 (w).

*Synthesis of* $Co(PO_3)_2$: Nanometer sized web-like $Co(PO_3)_2$ material was synthesized by thermal decomposition of **1** in a pressure reactor. An ethanol solution of **1** (ca. 0.5 mM, 15 mL) was placed in a Teflon-lined Parr Instrument 4744 general purpose pressure reactor, which was then sealed and placed in an oven heated to 240 °C for 8 h. The resulting material was removed from the reactor, washed with water, acetone, and ethanol multiple times with centrifugation. The resulting material was dispersed in ethanol or isopropanol (1 mg/mL) for working electrode fabrication.

## Supporting Information

Supporting Information is available from the Wiley Online Library or from the author.

## Acknowledgements

Funding for this work was provided by the Helios Solar Energy Research Center, which is supported by the Director, Office of Science, Office of Basic Energy Sciences of the U.S. Department of Energy under Contract No. DE-AC0205CH11231. The authors would like to acknowledge Professors A. Paul Alivisatos, Peidong Yang, and Alexis T. Bell for use of XRD, XPS, TEM and Raman instrumentation. The authors also thank Dr. Philip N. Ross for helpful discussions and advice.

Received: April 1, 2012
Revised: July 9, 2012
Published online: August 29, 2012

[1] N. S. Lewis, D. G. Nocera, *Proc. Nat. Acad. Sci. USA* **2006**, *103*, 15729.
[2] a) J. Kiwi, M. Grätzel, *Angew. Chem. Int. Ed.* **1978**, *17*, 860; b) J. M. Lehn, J. P. Sauvage, R. Ziessel, *Nouv. J. Chim.* **1980**, *4*, 355; c) A. Harriman, I. J. Pickering, J. M. Thomas, P. A. Christensen, *Chem. Soc. Faraday Trans. 1* **1988**, *84*, 2795.
[3] a) M. Hara, C. C. Waraksa, J. T. Lean, B. A. Lewis, T. E. Mallouk, *J. Phys. Chem. A* **2000**, *104*, 5275; b) M. Hara, J. T. Lean, T. E. Mallouk, *Chem. Mater.* **2001**, *13*, 4668; c) N. D. Morris, M. Suzuki, T. E. Mallouk, *J. Phys. Chem. A* **2004**, *108*, 9115; d) P. G. Hoertz, Y. I. Kim, W. J. Youngblood, T. E. Mallouk, *J. Phys. Chem. B* **2007**, *111*, 6845.
[4] a) T. Nakagawa, C. A. Beasley, R. W. Murray, *J. Phys. Chem. C* **2009**, *113*, 12958; b) T. Nakagawa, N. S. Bjorge, R. W. Murray, *J. Am. Chem. Soc.* **2009**, *131*, 15578.
[5] M. Yagi, E. Tomita, S. Sakita, T. Kuwabara, K. Nagai, *J. Phys. Chem. B* **2005**, *109*, 21489.
[6] a) J. F. Hull, D. Balcells, J. D. Blakemore, C. D. Incarvito, O. Eisenstein, G. W. Brudvig, R. H. Crabtree, *J. Am. Chem. Soc.* **2009**, *131*, 8730; b) J. D. Blakemore, N. D. Schley, D. Balcells, J. F. Hull, G. W. Olack, C. D. Incarvito, O. Eisenstein, G. W. Brudvig, R. H. Crabtree, *J. Am. Chem. Soc.* **2010**, *132*, 16017.
[7] N. C. King, C. Dickinson, W. Zhou, D. W. Bruce, *Dalton Trans.* **2005**, 1027.
[8] a) C. Sens, I. Romero, M. Rodríguez, A. Llobet, T. Parella, J. Benet-Buchholz, *J. Am. Chem. Soc.* **2004**, *126*, 7798; b) S. Romain,

F. Bozoglian, X. Sala, A. Llobet, *J. Am. Chem. Soc.* **2009**, *131*, 2768.

[9] a) L. Tong, L. Duan, Y. Xu, T. Privalov, L. Sun, *Angew. Chem. Int. Ed.* **2011**, *50*, 445; b) L. Duan, Y. Xu, P. Zhang, M. Wang, L. Sun, *Inorg. Chem.* **2010**, *49*, 209; c) Y. Xu, A. Fisher, L. Duan, L. Tong, E. Gabrielsson, B. Åkermark, L. Sun, *Angew. Chem. Int. Ed.* **2010**, *49*, 8934.

[10] a) J. J. Concepcion, J. W. Jurss, J. L. Templeton, T. J. Meyer, *J. Am. Chem. Soc.* **2008**, *130*, 16462; b) Z. F. Chen, J. J. Concepcion, J. W. Jurss, T. J. Meyer, *J. Am. Chem. Soc.* **2009**, *131*, 15580.

[11] B. S. Brunschwig, M. H. Chou, C. Creutz, P. Ghosh, N. Sutin, *J. Am. Chem. Soc.* **1983**, *105*, 4832.

[12] a) M. W. Kanan, D. G. Nocera, *Science* **2008**, *321*, 1072; b) Y. Surendranath, M. Dinc , D. G. Nocera, *J. Am. Chem. Soc.* **2009**, *131*, 2615; c) M. W. Kanan, Y. Surendranath, D. G. Nocera, *Chem. Soc. Rev.* **2009**, *38*, 109; d) Y. Surendranath, M. W. Kanan, D. G. Nocera, *J. Am. Chem. Soc.* **2010**, *132*, 16501; e) M. W. Kanan, J. Yano, Y. Surendranath, M. Dinc , V. K. Yachandra, D. G. Nocera, *J. Am. Chem. Soc.* **2010**, *132*, 13692; f) M. Risch, V. Khare, I. Zaharieva, L. Gerencser, P. Chernev, H. Dau, *J. Am. Chem. Soc.* **2009**, *131*, 6936; g) A. J. Esswein, Y. S. Surendranath, S. Y. Reece, D. G. Nocera, *Energy Environ. Sci.* **2011**, *4*, 499.

[13] a) D. K. Zhong, J. Sun, H. Inumaru, D. R. Gamelin, *J. Am. Chem. Soc.* **2009**, *131*, 6086; b) D. K. Zhong, D. R. Gamelin, *J. Am. Chem. Soc.* **2010**, *132*, 4202.

[14] a) E. M. P. Steinmiller, K. S. Choi, *Proc. Natl. Acad. Sci. USA* **2009**, *106*, 20633; b) J. A. Seabold, K. S. Choi, *Chem. Mater.* **2011**, *23*, 1105; c) K. J. McDonald, K. S. Choi, *Chem. Mater.* **2011**, *23*, 1686.

[15] a) J. B. Gerken, E. C. Landis, R. J. Hamers, S. S. Stahl, *ChemSusChem* **2010**, *3*, 1176; b) J. B. Gerken, J. G. McAlpin, J. Y. C. Chen, M. L. Rigsby, W. H. Casey, R. D. Britt, S. S. Stahl, *J. Am. Chem. Soc.* **2011**, *133*, 14431.

[16] F. Jiao, H. Frei, *Angew. Chem. Int. Ed.* **2009**, *48*, 1841.

[17] B. S. Yeo, A. T. Bell, *J. Am. Chem. Soc.* **2011**, *133*, 5587.

[18] a) A. J. Esswein, M. J. McMurdo, P. N. Ross, A. T. Bell, T. D. Tilley, *J. Phys. Chem. C* **2009**, *113*, 15068; b) N. H. Chou, P. N. Ross, A. T. Bell, T. D. Tilley, *ChemSusChem* **2011**, *4*, 1566.

[19] R. N. Singh, D. Mishra, A. S. K. Sinha, A. Singh, *Electrochem. Commun.* **2007**, *9*, 1369.

[20] a) Q. Yin, J. M. Tan, C. Bessen, Y. V. Geletii, D. G. Musaev, A. E. Kuznetsov, Z. Luo, K. I. Hardcastle, C. L. Hill, *Science*, **2010**, *328*, 342; b) Z. Huang, Z. Luo, Y. V. Geletii, J. W. Vickers, Q. Yin, D. Wu, Y. Hou, Y. Ding, J. Song, D. G. Musaev, C. L. Hill, T. Lian, *J. Am. Chem. Soc.* **2011**, *133*, 2068.

[21] a) J.-Z. Wu, F. D. Angelis, T. G. Carrell, G. P. A. Yap, J. Sheats, R. Car, G. C. Dismukes, *Inorg. Chem.* **2006**, *45*, 189; b) R. Brimblecombe, G. F. Wiegers, G. C. Dismukes, L. Spiccia, *Angew. Chem. Int. Ed.* **2008**, *47*, 7335; c) R. K. Hocking, R. Brimblecombe, L. Chang, A. Singh, M. H. Cheah, C. Glover, W. H. Casey, L. Spiccia, *Nat. Chem.* **2011**, *3*, 461.

[22] A. K. Poulsen, A. Rompel, C. J. McKenzie, *Angew. Chem. Int. Ed.* **2005**, *44*, 6916.

[23] a) K. W. Terry, C. G. Lugmair, T. D. Tilley, *J. Am. Chem. Soc.* **1997**, *119*, 9745; b) C. G. Lugmair, T. D. Tilley, A. L. Rheingold, *Chem. Mater.* **1997**, *9*, 339; c) C. G. Lugmair, T. D. Tilley, *Inorg. Chem.* **1998**, *37*, 6304; d) C. G. Lugmair, T. D. Tilley, A. L. Rheingold, *Chem. Mater.* **1999**, *11*, 1615; e) J. W. Kriesel, M. S. Sanders, T. D. Tilley, *Adv. Mater.* **2001**, *13*, 331; f) J. W. Kriesel, M. S. Sanders, T. D. Tilley, *Chem. Mater.* **2001**, *13*, 3554; g) K. L. Fujdala, T. D. Tilley, *J. Catal.* **2003**, *216*, 265; h) K. L. Fujdala, R. L. Brutchey, T. D. Tilley, in *Topics in Organometallic Chemistry*, Vol. *16* (Eds: C. Copéret, B. Chaudret), Springer-Verlag, New York **2005**, pp. 69–116.

[24] a) *Ultrastructure Processing of Advanced Materials*, (Eds: D. R. Uhlmann, D. R. Ulrich), Wiley-Interscience, New York **1992**; b) *Better Ceramics Through Chemistry V*, Materials Research Society Symposia Proceedings, Vol *271*, (Eds: M. J. Hampden-Smith, W. G. Klemperer, C. J. Brinker), Materials Research Society, Pittsburgh **1992**; c) *Inorganic Materials*, (Eds: D. W. Bruce, D. O'Hare), Wiley, New York **1992**; d) M. L. Kahn, A. Glaria, C. Pages, M. Mongo, L. S. Macary, A. Maisonnat, B. Chaudret, *J. Mater. Chem.* **2009**, *19*, 4044.

[25] a) R. Murugavel, M. Sathiyendiran, M. G. Walawalkar, *Inorg. Chem.* **2001**, *40*, 427; b) M. Sathiyendiran, R. Murugavel, *Inorg. Chem.* **2002**, *41*, 6404; c) R. Pothiraja, M. Sathiyendiran, R. J. Butcher, R. Murugavel, *Inorg. Chem.* **2004**, *43*, 7585; d) R. Murugavel, A. Choudhury, M. G. Walawalkar, R. Pothiraja, C. N. R. Rao, *Chem. Rev.* **2008**, *108*, 3549; e) R. Murugavel, N. Gogoi, *J. Organomet. Chem.* **2010**, *695*, 916.

[26] a) F. Meyer, R. Hempelmann, S. Mathur, M. Veith, *J. Mater. Chem.* **1999**, *9*, 1755; b) K. C. K. Swamy, M. Veith, V. Huch, S. Mathur, *Inorg. Chem.* **2003**, *42*, 5837.

[27] T. E. Gier, G. D. Stucky, *Nature* **1991**, *349*, 508.

[28] G. Cao, H.-G. Hong, T. E. Mallouk, *Acc. Chem. Res.* **1992**, *25*, 420.

[29] T. Kimura, *Microporous Mesoporous Mater* **2005**, *77*, 97.

[30] S. Brunauer, P. H. Emmett, E. Teller, *J. Am. Chem. Soc.* **1938**, *60*, 309.

[31] E. P. Barrett, L. G. Joyner, P. P. Halenda, *J. Am. Chem. Soc.* **1951**, *73*, 373.

[32] A. Zwierzak, M. Kluba, *Tetrahedron* **1971**, *27*, 3163.

[33] Y. Dong, K. He, L. Yin, A. Zhang, *Nanotechnology* **2007**, *18*, 435602.

[34] C. M. Taylor, S. P. Watson, P. A. Bryngelson, M. J. Maroney, *Inorg. Chem.* **2003**, *42*, 312.

[35] International Center for Diffraction Data "PDF-2", 2006; Card #27–1120.

[36] Given the inherent difficulty in determining gas adsorption surface areas for materials supported on Ni foam, electrochemically active surface areas were measured by the double layer capacitance method (see Supporting Information). Although this method involves certain assumptions that have raised questions regarding its applicability, it has been applied in studies of this kind, where electrode materials of a similar type are involved.

[37] A. J. Bard, L. R. Faulkner, *Electrochemical Methods: Fundamentals and Applications*, Wiley, New York **2001**, 103.

[38] a) M. Weil, M. Puchberger, J. A. Günne, J. Weber, *Chem. Mater.* **2007**, *19*, 5067; b) M. A. P. Silva, D. F. Franco, A. R. Brandão, H. Barud, F. A. Dias Filho, S. J. L. Ribeiro, Y. Messaddeq, L. F. C. de Oliveira, *Mater. Chem. Phys.* **2010**, *124*, 547.

[39] a) M. A. Vuurman, D. J. Stufken, A. Oskam, G. Deo, I. E. Wachs, *J. Chem. Soc. Faraday Trans.* **1996**, *92*, 3259; b) A. Boix, E. E. Miró, E. A. Lombardo, M. A. Bañares, R. Mariscal, J. L. G. Fierro, *J. Catal.* **2003**, *217*, 186; c) J. Yang, H. Liu, W. N. Martens, R. L. Frost, *J. Phys. Chem. C* **2010**, *114*, 111; d) R. K. Gupta, A. K. Sinha, B. N. Raja Sekhar, A. K. Sricastava, G. Singh, S. K. Deb, *Appl. Phys. A* **2011**, *103*, 13.

[40] S.-W. Ho, M. Houalla, D. M. Hercules, *J. Phys. Chem.* **1990**, *94*, 6396.

[41] *Handbook of X-ray Photoelectron Spectra: A Reference Book of Standard Spectra for Identification*, (Eds: K. D. Bomben, J. F. Moulder, P. E. Sobol, W. F. Stickel), Perkin Elmer, Eden Prairie **1992**.

[42] E. Deltombe, M. Pourbaix, *Atlas of Electrochemical Equilibria in Aqueous Solutions*, (Eds: M. Pourbaix), National Association of Corrosion, Houston **1974**, p. 504–515.

[43] The TOF for CoPi was reported in ref. 12d. It should be noted that the TOF for CoPi was determined based on the assumption that all Co in the sample is participating in catalysis, and thus represents an absolute lower limit. The value for $Co_3O_4$ was measured by the methods described above, and an example calculation is given in the Supporting Information.